Published in Surface Science 527, issues 1-3, 51-56, 2003
which should be used for any reference to this work

Growth of thin Bi films on W(1 1 0)

C. Koitzsch *, M. Bovet, F. Clerc, D. Naumović, L. Schlapbach, P. Aebi

Département de Physique, Université de Fribourg, Pérolles, CH-1700 Fribourg, Switzerland

Abstract

We report on the growth of single crystalline epitaxial Bi films on W(1 1 0). X-ray photoelectron diffraction (XPD) and low energy electron diffraction (LEED) reveal that Bi grows well ordered in the pseudocubic (0 0 1) orientation. The two-fold symmetric W(1 1 0) surface supports four different Bi(0 0 1) domains. The multi-domain nature is unambigously detected via LEED showing a peculiar splitting of spots. It is shown that a preferential domain alignment along the $[0\,0\,1]_{\text{tungsten}}$-direction accounts for this observation and is in agreement with a two-fold XPD pattern.

Keywords: Low energy electron diffraction (LEED); Photoelectron diffraction measurement; Growth; Tungsten; Bismuth

1. Introduction

Bismuth is a semimetal of the group V in the periodic table of elements with an atomic electron configuration of $[Xe]4f^{14}5d^{10}6s^26p^3$. It re-attracted considerable interest in the last years due to three effects. The discovery of superconductivity in small granular clusters [1] despite the non-superconducting properties for bulk Bi opened the question of the surface electronic structure being responsible for the superconducting state. Secondly, the electronic properties of Bi make it almost an ideal candidate to study quantization phenomena, the Fermi wave vector with experimentally convenient dimensions of the order several nm. Quantum size effects should render thin films insulating due to a thickness induced quantization of the valence band [2] and a subsequent lifting of the overlap between electron and hole bands at E_F. Furthermore the large $Z = 83$ should give rise to a considerable effect of the spin-orbit interaction on the valence band structure, namely the p-bands and surface localized states in the vicinity of the Fermi level [3–5].

In this work we report on the growth of thin Bi films on W(1 1 0). To our knowledge, this is the first time, that Bi growth on this substrate is reported. Tungsten was chosen as a substrate since it is a refractory metal, and hence does not alloy with Bi. Furthermore its large band gaps [6] of the projected bulk band structure in certain regions of the surface Brillouin zone make it a suitable substrate for studies of ultra thin films because a clear separation between substrate and film valence states is feasible. The present study shows that well ordered single crystalline films can be obtained via room temperature growth on W(1 1 0). It is demonstrated that these films grow in a multi-domain fashion in the pseudocubic [1 0 0]-orientation.

* Corresponding author.

2. Experimental details

The preparation of clean W(1 1 0) surfaces has already been described elsewhere [7]. The crucial step in order to deplete the crystal from C was a 125 h anneal at 1500 K under an oxygen partial pressure of 10^{-7}mbar. Subsequently an unreconstructed surface, free of surface contaminants can be obtained by flashing the crystal via e-beam heating up to 2500 K in ultra high vacuum. Bi was deposited at room temperature out of a water cooled home built evaporator at a rate of approximately 2 Å/min, as measured by an oscillating quartz crystal. The pressure during deposition did not exceed 2×10^{-10} mbar. The crystal structure was monitored by low energy electron diffraction (LEED), snapshots of the diffraction pattern were made with an 8-bit CCD camera.

The photoemission experiments were performed in situ in a modified VG Mk II spectrometer equipped with a two-axis sample goniometer enabling sequential computer-controlled sample rotation [8,9]. For X-ray photoelectron diffraction (XPD) a twin anode was used delivering MgKα radiation ($h\nu = 1253.6$ eV). The angular resolution was 1° full cone acceptance. It has been shown that full hemispherical XPD patterns (diffractograms) provide very direct information about the near surface structure. Its chemical sensitivity and the sensitivity to local order render it a powerful method for structural investigations [10]. At electron energies above 500 eV, the anisotropic scattering of photoelectrons by the ion cores leads to a forward focusing of electron flux along the emitter-scatterer axis. Prominent intensity maxima in diffractograms can often be immediately identified with near-neighbour directions. The chemical sensitivity arises from diffractograms of different core levels, allowing for the determination of local order around specific atomic species, for a review on XPD see Ref. [11]. Here XPD patterns from W and Bi 4f core levels are shown. The obtained angular distributions of intensities, projected stereographically, are plotted in a linear grey scale image.

Furthermore we present simulations of the aforementioned XPD pattern. These simulations are based on model clusters (see below), where for every constituent atom the corresponding forward focusing maxima arising from the surrounding atom ensemble are calculated. For a given example atom, intensity maxima are found in direct line of sight between the example atom, which can be viewed as emitter and the surrounding atoms, which are the scatterers. The dot-size for each forward focusing event is inversely proportional to the distance between emitter and scatterer.

3. Results and discussion

Since crystal growth is the main focus of the present paper a short insight into the lattice properties of bulk Bi is given. Bismuth has a reported bulk lattice constant of 4.75 Å. The crystal structure is rhombohedral with space group 166. This rhombohedral lattice can be understood as distorted cubic [12]. A rhombohedral unit cell with a shear angle of 60° and a two atom basis, where the second basis atom is centered can equally be described with a simple cubic lattice. Fig. 1(a) shows this relationship, while in Fig. 1(b) a (1 1 0)-plane of the tungsten crystal is depicted. For the present case of Bi, the shear angle is 57.35° and the basis atom positions are (0,0,0) and (0.474, 0.474, 0.474). This introduces small distortions, resulting for the (0 0 1) surface in a rectangular surface unit cell with the two unit cell vectors not equal and a two-atom basis [5]. The resulting lattice is called pseudocubic. In the following we will refer to the crystallographic directions in pseudocubic coordinates.

In Fig. 2 two LEED pictures are shown, which illustrate the changes, when thin bismuth films are deposited. The principal crystallographic directions for W(1 1 0) are indicated in (a) and the orientation of the W(1 1 0) crystal below the Bi film in (b) is identical.

Based on LEED, we can already derive the orientational relationship between the reciprocal lattices of substrate and film. The surface unit cell of bismuth films, indicated in Fig. 2(b), appears oriented approximately 45° off with respect to the W(1 1 0) surface unit cell (Fig. 2(a)). The lengths of the reciprocal unit cell vectors (Fig. 2(a)) yield the expected real space bulk values for W(1 1 0), which

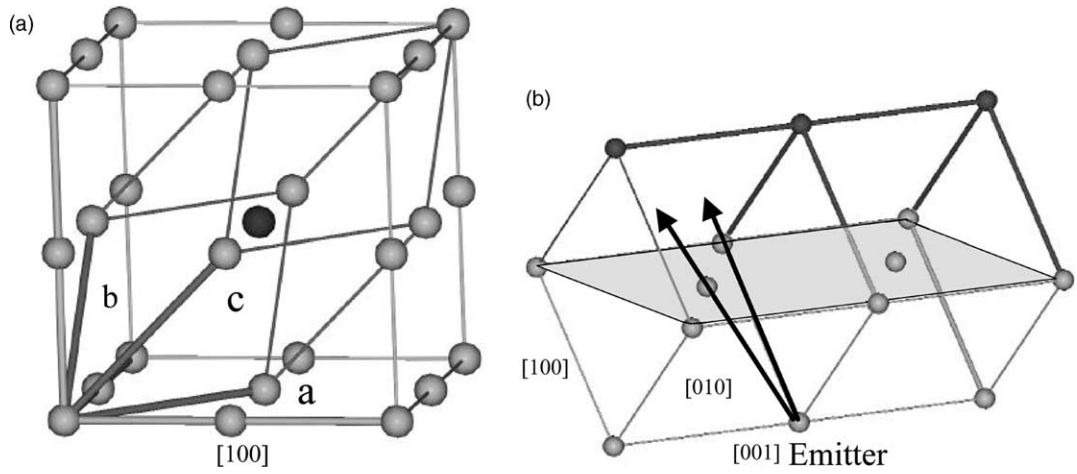

Fig. 1. (a) Simple cubic lattice with rhombohedral unit cell inscribed, the second basis atom is shaded in black, the pseudo-cubic unit cell vectors are along the cube edges, the [1 0 0] growth direction is indicated. (b) Cut through a bcc tungsten unit cell, the (1 1 0) surface is shaded, principal forward focusing directions from one emitter atom are indicated by arrows (see text).

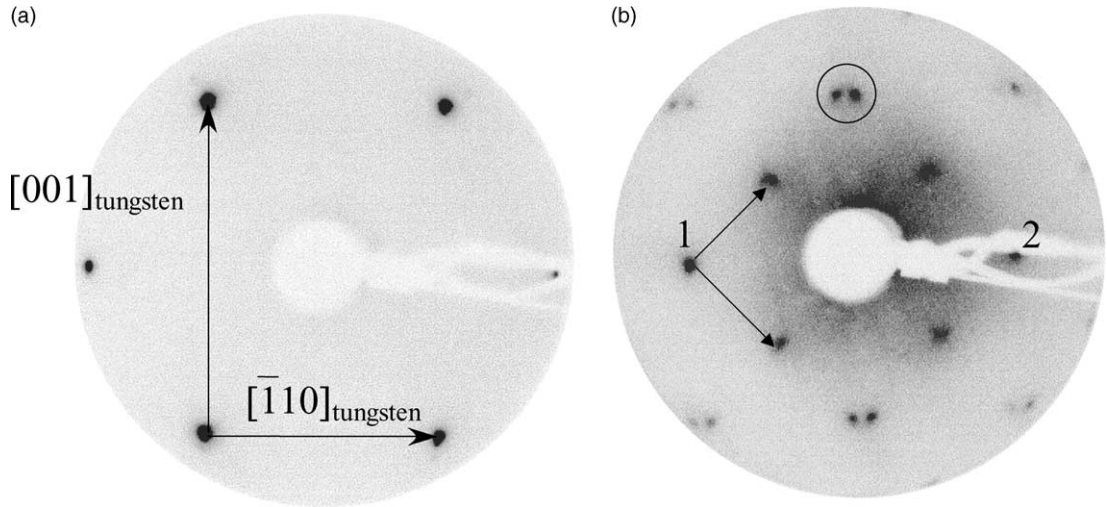

Fig. 2. LEED pictures, $E_{\text{beam}} = 61.3$ eV, for (a) clean W(1 1 0), (b) a nominal Bi coverage of 70 Å.

has a lattice constant of 3.165 Å [15]. For the Bi film (Fig. 2(b)) a pseudo-cubic surface unit cell is obtained, which suggests a (0 0 1)-orientation. This symmetry excludes immediately the [1 1 1]-direction, since the [1 1 1]-direction is a trigonal axis. This is a somewhat surprising result, since a variety of other metals deposited on W(1 1 0) grow along the [1 1 1]-direction [13,14]. The length of the reciprocal unit cell vectors (Fig. 2(b)) translates into a rectangular real space unit cell with a length of 4.3 ± 0.3 and 4.6 ± 0.3 Å. This is to be compared to Bi bulk values of 4.53 and 4.75 Å [15].

A peculiar doubling of spots (circled in Fig. 2(b)) appears for all observed spots except the ones lying on a horizontal line across the center of the image. The diffraction spots without splitting are marked with numbers 1 and 2 in Fig. 2(b). In order to understand the origin of the observed spot

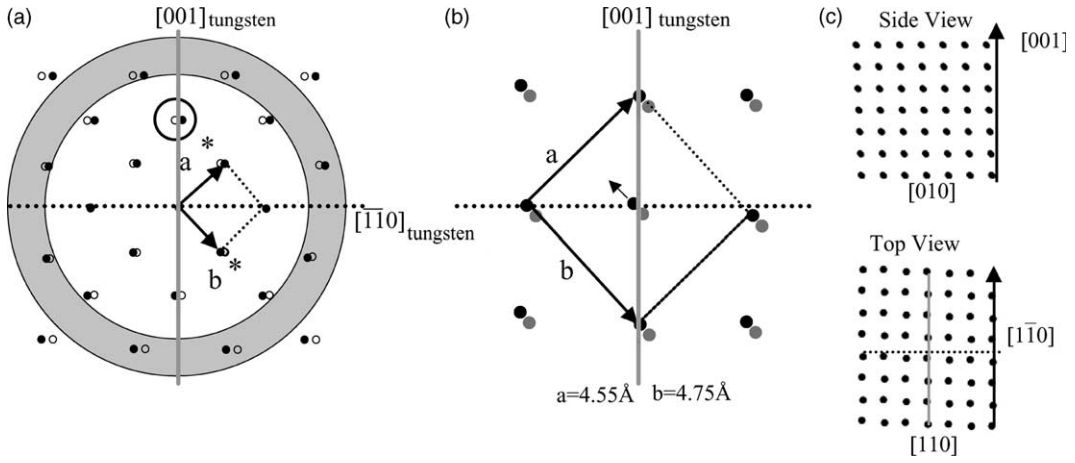

Fig. 3. (a) Reciprocal Bi(0 0 1) surface net shown in black dots, mirror domain shown in open circles; the circle illustrates the field of view for the LEED experiments; reciprocal unit cell vectors are denoted as a* and b*. (b) Real space surface net drawn in black dots; shown in grey is a buried Bi layer illustrating the pseudo-cubic stacking; the second basis atom (marked by an arrow) is shifted away from the center. (c) Global view on the resulting cluster; the top view shows the alignment to the $[0\,0\,1]_{\text{tungsten}}$-direction and the sideview illustrates the formation of atomic rows, which are tilted away from the surface normal.

splitting, the reciprocal surface lattice for the suggested (0 0 1) orientation was calculated and is shown in Fig. 3(a) with black dots. Additionally in Fig. 3(a) the same reciprocal lattice is shown but after a mirror operation (open circles in Fig. 3(a)) as explained below. The field of view, as indicated by the shaded circle is adapted to the experimental LEED geometry and the region, where no spot splitting occurs is marked by a black dotted line. Already one notices a very good agreement between the experimental LEED pattern and the combined pattern of the two reciprocal surface nets (black and open circles in Fig. 3(a)). The two reciprocal lattices are interrelated by mirror symmetry with mirror axis either the $[\bar{1}\,1\,0]_{\text{tungsten}}$ or $[0\,0\,1]_{\text{tungsten}}$-direction. The reason why only some spots appear split, is the alignment of the reciprocal unit cell diagonal along the $[\bar{1}\,1\,0]_{\text{tungsten}}$-direction. The $[\bar{1}\,1\,0]_{\text{tungsten}}$-direction is the alignment axis for the reciprocal unit cell diagonal and they both are found on the black dotted line in Fig. 3(a). All spots, which can be found on this alignment axis, will not appear split, for a mirror axis, which is either the alignment axis itself or an axis oriented perpendicular to the alignment axis (grey line in Fig. 3(a)). The observed LEED pattern therefore supports the existence of mirror domains, which are related to the original domain (black circles in Fig. 3(a)) via the $[\bar{1}\,1\,0]_{\text{tungsten}}$ or $[0\,0\,1]_{\text{tungsten}}$ mirror axis. Fig. 3(b) shows the corresponding real space atom ensemble, the topmost Bi layer is shown in black dots, a second layer deeper in the bulk is shown in grey dots. The crystal is aligned such that the corresponding reciprocal net is aligned in the aforementioned manner. One immediately notices that in real space the unit cell diagonal is aligned along the $[0\,0\,1]_{\text{tungsten}}$-direction (grey line in Fig. 3(b)), exactly perpendicular to the alignment direction in reciprocal space. The observed LEED pattern has to be therefore interpreted, such that the $[0\,0\,1]_{\text{tungsten}}$ is the principal alignment axis with the formation of atom rows as shown in Fig. 3(b) along this direction.

The formation of atom rows along the $[0\,0\,1]_{\text{tungsten}}$-direction could suggest a particularly good match between substrate and film along this direction. Indeed it is comparable to the lattice matching for [1 1 1]-oriented metals, which usually grow in the Nishiyama–Wassermann relation [16] on W(1 1 0). In this epitaxial relation one has an alignment between the $[0\,0\,1]_{\text{tungsten}}$-direction and the hexagonal $[2\,\overline{1}\,\overline{1}\,0]$-direction with a possible supercell commensuration in this direction. Ap-

parently for the case of Bi an arrangement in [0 0 1]-direction offers an advantage in terms of lattice match, one obtains based on the Bi bulk crystal structure a lattice misfit of only 3.6% in the $[0\,0\,1]_{\text{tungsten}}$-direction.

Fig. 3(c) shows a more global view of the crystallographic arrangement of a Bi cluster oriented in the aforementioned manner in (a) sideview and (b) top view. Note the formation of atom rows, which have a small tilt away from the [1 0 0] surface normal (see below). This tilt is especially apparent in Fig. 3(c) as an opening angle between the [0 0 1]-direction (surface normal) and the atomic row right beside it.

The real space crystallographic structure can be determined by XPD. Here, additionally, the out-of-plane structure is accessible. We measured the angular dependence of the photoelectron signal for W and Bi 4f core level emission. The corresponding emission patterns in stereographic projection, are shown in Fig. 4(a,b). For W(1 1 0) (Fig. 4(a)) we notice a two-fold symmetry with the strongest emission maxima at polar angles of 35° and 45°. Their relationship to the real space structure becomes obvious if emission from a sub-surface site (Fig. 1(b)), is considered. Here, forward focusing from this emission site due to scattering at the very surface layer is expected for polar angles with respect to the [1 1 0] surface normal of 45° in [1 0 0]-direction and 35° in [1 1 1]-direction. All resulting foward focusing maxima, based on a cluster are shown as an overlay in the lower half of the W 4f emission pattern. Note, that densely packed crystallographic planes appear as high intensity bands, known as Kikuchi bands [17]. In a stereographic projection planes appear as circular segments or straight lines for the ones containing the sample normal.

Regarding the a priori unknown crystalline orientation of the Bi film one has to rely on already known crystal structure data and the symmetry of the pattern (Fig. 4b) in order to simulate the experimental situation. The pattern is nearly four-fold symmetric, with slightly differently shaped straight (circled features in Fig. 4b numbered one and two) Kikuchi bands along the $[0\,0\,1]_{\text{tungsten}}$ and $[\bar{1}\,1\,0]_{\text{tungsten}}$-direction, rendering it two-fold symmetric. Primary forward-focusing peaks are marked by a circle in Fig. 4(b) and labeled with numbers three and four. In order to facilitate a more

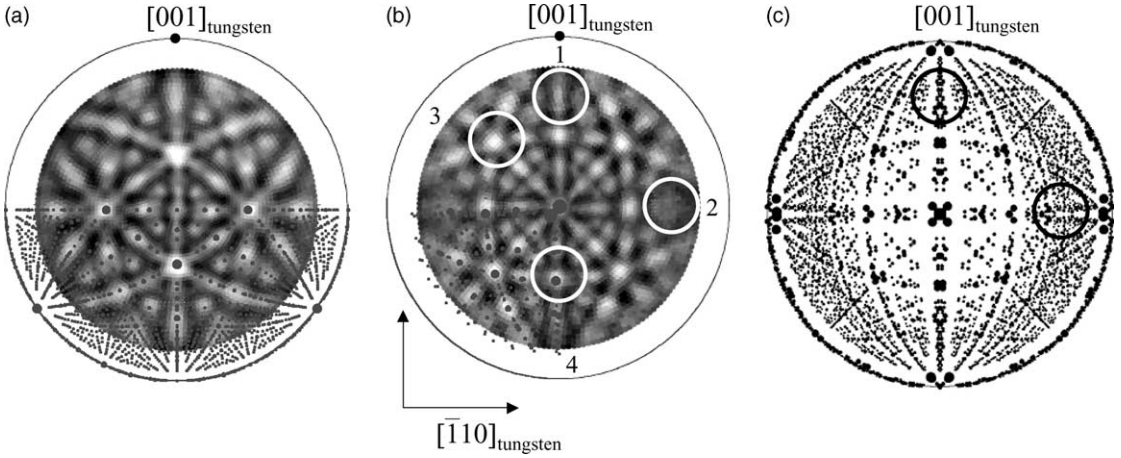

Fig. 4. MgKα excited XPD, the center corresponds to normal emission, while the outer circle corresponds to an emission angle of 90° with respect to the surface normal. The diffractograms are plotted in a linear grey scale with high intensity shown in white (a). Diffractogram from the clean W(1 1 0) substrate showing the angular dependence of the W 4f level $E_{\text{kinetic}} = 1222$ eV and the result of a cluster calculation as overlay. (b) Bi 4f diffractogram, $E_{\text{kinetic}} = 1097$ eV, and forward focusing direction for one domain as overlay; circled regions one and two render the XPD pattern twofold symmetric, circled regions three and four are primary forward focusing peaks centered at polar angles of 56.2° (feature three) and 45.8° (feature four). The observed forward focusing peaks are within the experimental error at their theoretical position of 56.4° and 45°. (c) Forward focusing directions based on a pseudo-cubic cluster and three mirror domains.

in-depth understanding of the diffractogram, forward focusing directions based on a (0 0 1) oriented pseudo-cubic Bi cluster (Fig. 3(c)) were determined. The calculation bases on a cluster which is rotated such that the real space unit cell diagonal (Fig. 3b) is aligned to the $[0\,0\,1]_{\text{tungsten}}$-direction, in accordance with the LEED spot splitting.

The resulting forward focusing directions (overlay in Fig. 4(b)) are in very good agreement with the experimental pattern, which in general confirms the [1 0 0] growth direction. Nevertheless the calculated pattern is not two-fold symmetric, a fact which is easily seen for forward focusing around the surface normal. In this region the calculation yields two features, which render the diffractogram one-fold symmetric. The reason for this low symmetry is the crystal structure of Bi itself (Fig. 3(c)). The pseudo-cubic nature of Bi leads to atom rows slightly tilted away from the pseudo-cubic [1 0 0]-direction, which is the wobble away from the surface normal (Fig. 3c). The two-fold symmetry must then originate from different domains, an assumption which has already been used to explain the LEED spot splitting. Fig. 4(c) shows again the stereographic projection of forward focusing directions, but in addition the results from mirror clusters. Now the two-fold symmetry is nicely reproduced, the stronger Kikuchi line along $[0\,0\,1]_{\text{tungsten}}$ is clearly visible (circled features in Fig. 4(c)), again confirming the multi-domain nature of Bi films on W(1 1 0).

4. Conclusions

It has been shown that the combination of LEED and XPD allows for an in-depth determination of the crystal structure of Bi thin films on W(1 1 0). Four different growth domains, along with a diagonal alignment of the Bi surface unit cell parallel to $[0\,0\,1]_{\text{tungsten}}$-direction, explains both the doubling of LEED spots and the two-fold symmetry of the XPD pattern. The obtained good crystalline quality of the films on W(1 1 0) render subsequent investigations of e.g. quantum size effects, spin-orbit coupling etc. with various techniques very promising.

Acknowledgements

We are greatly indebted to our workshop and electric engineering team, including O. Raetzo, E. Moser, R. Schmid, R. Vonlanthen, Ch. Neururer, and F. Bourqui. Financial support by the Fonds National Suisse pour la Recherche Scientifique is gratefully acknowledged.

References

[1] B. Weitzel, H. Micklitz, Phys. Rev. Lett. 66 (1991) 385.
[2] V. de Renzi, M.G. Betti, C. Mariani, Phys. Rev. B 48 (1993) 4467.
[3] M. Hengsberger, P. Segovia, M. Garnier, D. Purdie, Y. Baer, Eur. Phys. J. B 17 (2000) 603.
[4] C.R. Ast, H. Höchst, Phys. Rev. Lett. 87 (2001) 177602.
[5] S. Agergaard, C. Sondergaard, H. Li, M.B. Nielsen, S.V. Hoffmann, Z. Li, Ph. Hofmann, New J. Phys. 3 (2001) 15.1.
[6] A.M. Shikin, D.V. Vyalikh, G.V. Prudnikova, V.K. Adamchuk, Surf. Sci. 487 (2001) 135.
[7] J. Hayoz, Th. Pillo, A. Züttel, St. Guthrie, P. Aebi, L. Schlapbach, J. Vac. Sci. Technol. A 18 (5) (2000) 2417.
[8] J. Osterwalder, T. Greber, A. Stuck, L. Schlapbach, Phys. Rev. B 44 (1991) 13764.
[9] D. Naumović, A. Stuck, T. Greber, J. Osterwalder, L. Schlapbach, Phys. Rev. B 47 (1993) 7462.
[10] Th. Pillo, J. Hayoz, P. Schwaller, H. Berger, P. Aebi, L. Schlapbach, Appl. Phys. Lett. 75 (1999) 1550.
[11] C.S. Fadley, in: R.Z. Bachrach (Ed.), Synchrotron Radiation Research: Advances in Surface Science, Vol. 1, Plenum, New York, 1990, pp. 421–518.
[12] F. Jona, Surf. Sci. 8 (1967) 57.
[13] e.g. YH_x: J. Hayoz, S. Sarbach, E. Boschung, D. Naumović, P. Aebi, L. Schlapbach, Phys. Rev. B 58 (1198) R4270.
[14] e.g. Ag, Au: A.M. Shikin, D.V. Vyalikh, Yu.S. Dedkov, G.V. Prudnikova, V.K. Adamchuk, E. Weschke, G. Kaindl, Phys. Rev. B 62 (2000) R2303.
[15] Pearson's Handbook of Crystallographic Data for Intermetallic Phases, P. Villars, L.D. Calvert, American Society for Metals, Metals Park, OH 44073.
[16] E. Bauer, Appl. Surf. Sci. 11/12 (1982) 479.
[17] R. Trehan, J. Osterwalder, C.S. Fadley, J. Electr. Spectr. Rel. Phenomena 42 (1987) 187.